Int. J. Electrochem. Sci., 16 **(2021)** Article ID: 210328, doi: 10.20964/20201.03.13

International Journal of
ELECTROCHEMICAL
SCIENCE
www.electrochemsci.org

Short Communication

Synthesis of ZIF-67@ZIF-8 with Core-shell Structure for Enhancing Epoxy Coating Corrosion Protection Property on Magnesium Alloy

Kun Cao[1], Leilei Yu[1], Xinlan Liu[1], Yanqiu Yang[1], Fubin Ma[2,]*

[1] Department of Chemistry & Chemical Engineering, Neijiang Normal University, Neijiang, Sichuan, 641112, PR China
[2] Institute of Oceanology, Chinese Academy of Sciences, Qingdao, 266000, China
[*]E-mail: kevin_cao0811@126.com

Received: 1 November 2020 / *Accepted:* 14 December 2020 / *Published:* 31 January 2021

Nanocontainers with corrosion inhibitors are an effective means to protect metals from corrosion. However, such coatings need to release the inhibitors rapidly to form an on-demand barrier on the metal surface, whereas coating damage needs to be minimized to prevent excessive leakage. Herein , this function is achieved by ZIF-67@ZIF-8 nanoparticles, a metal organic frame material with core-shell structure, by acting as a functional filler. The structure and composition of ZIF-67 and ZIF-67@ZIF-8 nanoparticles are assessed by TEM, SEM and XRD. The findings of UV spectroscopy and immersion experiments show that ZIF-67@ZIF-8 nanoparticles rapidly release 2-MI to the damaged area of the metal surface in acid conditions. In addition, in a neutral environment, only limited amounts of 2-MI (less than 4%) are released. The coating has high corrosion resistance after immersion for 120 h in acidic condition, as exhibited by EIS, and thus potential application value.

Keywords: core-shell structure; metal organic framework; ZIF-67@ZIF-8; anticorrosion coating

1. INTRODUCTION

Magnesium and its alloys are ideal materials for the developing engineering materials for use in multiple areas, such as the automobile industry, aerospace, and infrastructure, primarily due to their high strength-to-weight ratio, low density, and easy recyclability [1–4]. However, in the aqueous conditions, magnesium shows almost no corrosion resistance which restricts its applications[5-10]. Surface coating is among the most effective ways to avoid corrosion of highly electrochemically active magnesium and its alloys. Organic or hybrid coatings allow long-lasting protection of the surface without damaging the mechanical properties of this light weigh metal construction.

Epoxy coatings are an effective choice to protect the Mg alloy surface against corrosion, owing

to the low water penetration rate of the epoxy layer and its high adhesion to the substrate. Nevertheless, due to inherent structural defects of the coating itself, corrosion particles can penetrate the coating and reach the coating/substrate interface, Therefore, organic coatings are not permanently impermeable organic coating [11,12]. At the same time, when the corrosion particles reach the coating / substrate interface, a large amount of corrosion products will cause the coating to peel off and then degrade [13]. Anticorrosion properties may be maintained against damage by endowing the self-healing coatings. The widely used technique for self-healing coatings is the integration of self-healing reagents into coatings. After damage of the coatings, the self-healing reagents are released to repair the damages.

Metal organic frameworks (MOFs) are a novel form of multifunctional crystal hybrid material, and have been widely used in the fields of chemical sensors, gas storage, molecular recognition and heterogeneous catalysis [14-17]. For example, three-dimensional MOFs are used as drug delivery carriers via loaded the drug into porous MOFs and are released in a regulated manner in a specific target area (e.g. acidic environment in tumors)

In this paper, we prepared core-shell ZIFs by epitaxial growth. In addition to being a strong inhibitor to improve the coating's corrosion resistance, the organic ligand also retains the stability of the coating and prevents the leakage of the corrosion inhibitor from the nanocontainer. On-demand release of corrosion inhibitors in core-shell ZIFs at various pH values has been examined. Forthermore, electrochemical impedance spectroscopy (EIS) findings suggested that the self-healing coating provided effective corrosion protection.

2. EXPERIMENTAL

2.1 Materials and chemicals

The following materials have been acquired from Sinopharm Chemical Reagent Co., Ltd: cobalt nitrate ($CoNO_3 \cdot 6H_2O$), zinc acetate [$(CH_3COO)_2Zn$], 2-methylimidazole (2-MI) and methanol. The epoxy emulsion (H228A) and its curing agent (H228B) used in this research were supplied by Shanghai Hi-Zone Chemical Factory. A water purification machine was used for producing deionized (DI) water.

2.2 Synthesis of ZIF-67@ZIF-8

ZIF-67 was synthesized from a methanol solution of $CoNO_3$ (4 mmol, 10 ml) and 2-methylimidazole (160 mmol, 200 ml), that were stirred for at room temperature 24 h. After centrifugation and washing twice with ethanol solution, the product was directly used as seed without drying. ZIF-67 was dispersed in 80 mL of a methanol solution of 16 mmol 2-methylimidazole, followed by stirring for 5 min, then 20ml of a methanol solution of 4 mmol $(CH_3COO)_2Zn$ were added, and stirring was continued at room temperature for 1 h, followed by standing for 24 h. ZIF-67@ZIF-8 was obtained as the final product by centrifugation, rinsed twice with ethanol, and dried for 12 h in a vacuum at 50 °C.

2.3 Coating preparation

First, 100 mg of ZIF-67@ZIF-8 nanocontainers were introduced to the epoxy resin, followed by stirring and ultrasound dispersion for 60 min to produce a homogeneous dispersion system. The coatings were then formed via dip coating on AZ31B sheets three times. The thickness of the coating on AZ31B was maintained in the 28-30 μm range while using a thickness tester (Qnix 8500, Germany).

2.4 Characterization

Transmission electron microscopy (TEM, HT-7700, Hitachi, Japan) with a voltage of 100 kV and scanning electron microscopy (SEM, SU 8010, Hitachi, Japan) with a voltage of 5.0 kV were used to observe the morphologies of the nanocomposites. XRD patterns were obtained using the Cu Kα radiation source (λ=1.5406 Å) on a Rigaku Ultimate VI X-ray diffractometer (40 kV, 20 mA). UV–vis spectroscopy was used to analyze the concentration of released 2-MI in an aqueous solution. (TU-1901, Purkinje General, China)

2.5 2-MI released from ZIF-67@ZIF-8

The release of 2-MI from ZIF-67@ZIF-8 at different pH values was studied by UV–vis spectroscopy. For this purpose, 0.1 g ZIF-67@ZIF-8 was dispersed in a 50 mL HCl solution at different pH values (pH = 1, 2, 3 and 6.8), and the resulting solution was stirred at 500 rpm at 25 °C. After a certain time, 100 μL solution aliquots were obtained, filtered through a 0.22 μm microporous cellulose membrane, and diluted accordingly. Then, release profiles were acquired by plotting the absorbance of 2-MI in the solution at the wavelength of 440 nm as a function of the time.

2.6 Corrosion performance evaluation

Electrochemical impedance spectroscopy (EIS) on an Ivium electrochemical workstation was used to examine the coated samples' corrosion resistance. A three-electrode system was employed with a 1 M HCl aqueous solution as the electrolyte, a Pt foil as counter electrode, and an Ag/AgCl electrode as a reference electrode. The EIS was carried in10^5 to 10^{-2} Hz frequency range with 10 mV amplitude and an open circuit potential (OCP). To shorten the test period, an evaluation of the corrosion performance was also carried out base on an accelerated corrosion test, The AZ31B modified with a pure epoxy coating or the addition of ZIF-67@ZIF-8 was deliberately scratched about 1 cm long and with 40 μm wide using a surgical knife, preceded by immersion in 1 M HCl aqueous solution.

3. RESULTS AND DISCUSSION

3.1 Synthesis and characterization of ZIF-67@ ZIF-8 nanoparticles

As indicated in Fig. 1, ZIF-67 crystal particles with smaller size were synthesized from methanol

solution of cobalt nitrate and 2-methylimidazole according to a method adopted in this experiment [18]. As ZIF-8 crystals have characteristics of slow nucleation rate ZIF-8 crystals of large size can be easily obtained. ZIF-8 crystals with larger size were obtained by using a lower concentrated methanol solution of zinc acetate tetrahydrate, as a low ligand concentration hinders nucleation and crystal growth, and the coordination strength between metal ions and acetate ions is greater than that between metal ions and nitrate ions, which increases the crystal growth stage to a certain extent. To obtain ZIF-8 crystals with larger size, ZIF-67 crystals with smaller size were used as crystal seed, and a methanol solution of zinc acetate tetrahydrate was added to control the reaction conditions toward the formation of larger size crystals. Then, the shell layer was formed to obtain ZIF-67@ZIF-8 crystal particles as uniform crystal particles with core-shell structure. The SEM analysis showed that the collected ZIF-67@ZIF-8 core-shell crystals were rhombic dodecahedrons with uniform particle size. Fig. 1 indicates that the seeds with a very smooth surface and comparatively larger particle size had the same morphology as the core-shell crystals. Moreover, owing to the identical topology and homogenous unit cell parameters of ZIF-67 and ZIF-8 [19,20], similar X-ray diffraction (XRD) patterns were recorded for the acquired ZIF-67 and ZIF-8 containing core-shell crystals, which were nearly the same as the simulated XRD patterns of the ZIF-67 crystals (Fig. 2). All these results indicate that the epitaxial growth process has successfully produced the core-shell crystals.

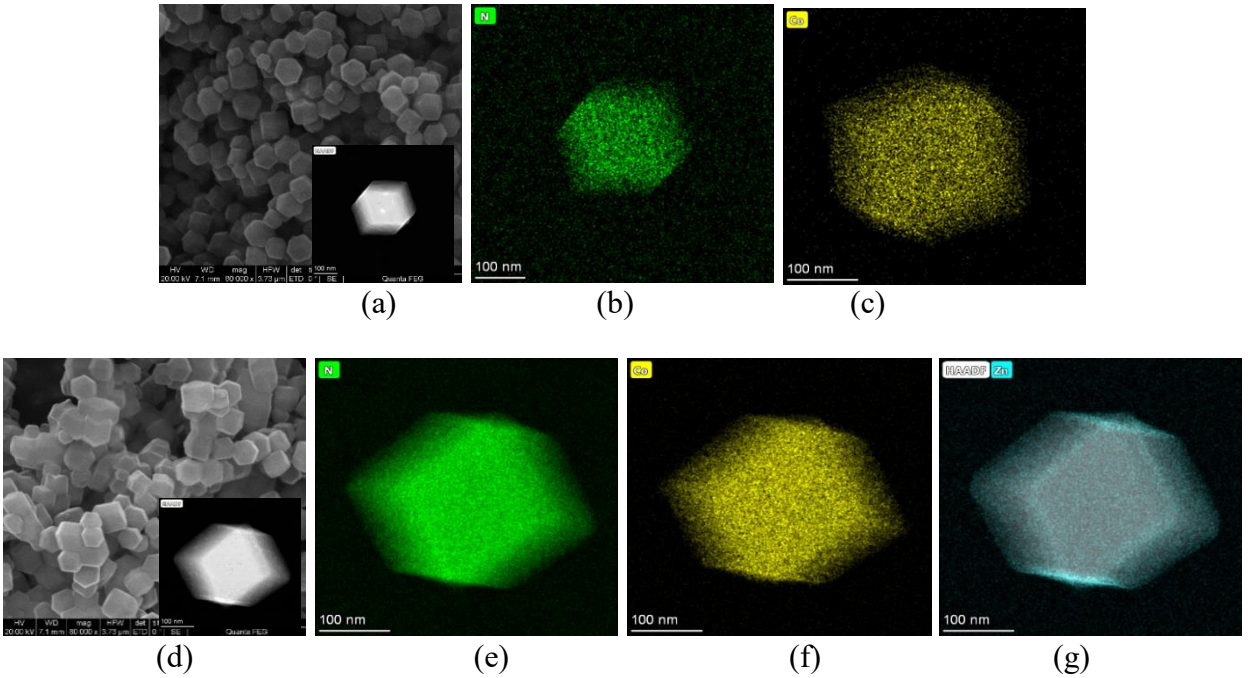

Figure 1. SEM images, TEM images and elemental mappings of core-shell ZIF-67 crystals (a, b, c) and core-shell ZIF-67@ZIF-8 crystals (d, e, f, g)

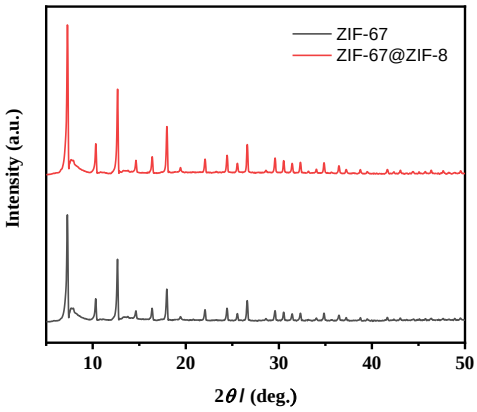

Figure 2. XRD patterns of ZIF-67 and core-shell ZIF-67@ZIF-8 crystals

3.2 pH-responsive release and inhibitory properties of ZIF-67@ZIF-8 nanoparticles

The ZIF-67@ZIF-8 nanoparticles release behavior was studied at diverse pH values in 1-6.8 range. Fig. 3 displays the kinetics of the effective release of the ZIF-67@ZIF-8 nanoparticles. The results show that they are obviouslyclearly sensitive to acidic pH conditions. In a neutral environment, the. The amount of the released 2-methylimidazole released in a neutral environment was lowerless than 4 wt %,percent by weight, which was attributeddue to the stability of thestable metal ion－ligand coordination bond [21]. At pH=1, 40.6 wt percent of 2-MI was released quickly(within 20 min) from ZIF-67@ZIF-8, resulting in the separation of the MOFs [22, 23]. Nevertheless, with a rise in pH, the capacity of the ZIF-67@ZIF-8 nanoparticles to release inhibitor molecules reduced continuously . The as-synthesized ZIF-67@ZIF-8 nanoparticles are a candidate for carriers with the rapid and pH-dependent release of a large amounts of inhibitors while preventing undesirable deterioration of the coating in a neutral environment.

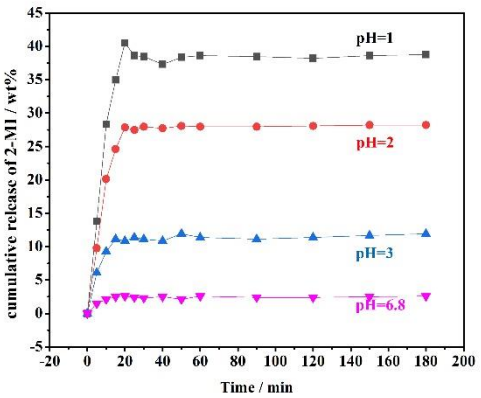

Figure 3. Cumulative release of 2-MI from ZIF-67@ZIF-8 nanoparticles at different pH (1, 2, 3 and 6.8)

3.3 Anticorrosive properties of the coating

EIS examined the corrosion resistance of the coating. Samples were immersed in corrosive medium at different times to form coatings containing different ZIF derivatives (epoxy-ZIF-67 and epoxy-ZIF-67@ZIF-8). To cause corrosion and evaluateto test the corrosion resistance of AZ31B magnesium alloy to corrosion resistance, the AZ31B alloy was exposed to the electrolyte, and the scratches with a length of sharp knife, 1 cm long and a width of 40 μm wide marks were artificially made with a sharp knifedeliberately produced. The Nyquist plots shown in Fig. 4, demonstrate the progress of the corrosion in the coating system with the time. During the whole corrosion process, EIS exhibited a much better corrosion resistance for the nanocomposite coating than for the control coating. EIS exhibited a much better corrosion resistance for the nanocomposite coating than for the control coating. Using the equivalent circuit, shown in Fig. 5 with two time-constants, charge transfer resistance R_{ct}, coating resistance R_c, coating capacitance CPEc and electrolyte resistance R_s of AZ31B were extracted from its EIS spectra. Based on prior research, high R_{ct} and low CPEc are related to coatings with a good anticorrosion ability, as R_{ct} demonstrates the resistance to aggressive species transfer, and CPEc is tendency of coating to absorb water. After incubation for 120 h in 1 M HCl solution, the epoxy coating with ZIF-67@ZIF-8 exhibited R_{ct} and CPEc values of 9.5×10^5 Ω·cm^2 and 94.3 μF/cm^2, which were 4.3 times higher and 3.3 times lower than those of the pure epoxy coating (2.2×10^5 Ω·cm^2 and 312.2 μF/cm^2), respectively. This suggested that the epoxy coating with ZIF-67@ZIF-8 prevents the water absorption of coating, which can be due to the adsorption of 2-MI, confirming that the addition of core-shell ZIFs further improves the barrier performance of the coating.

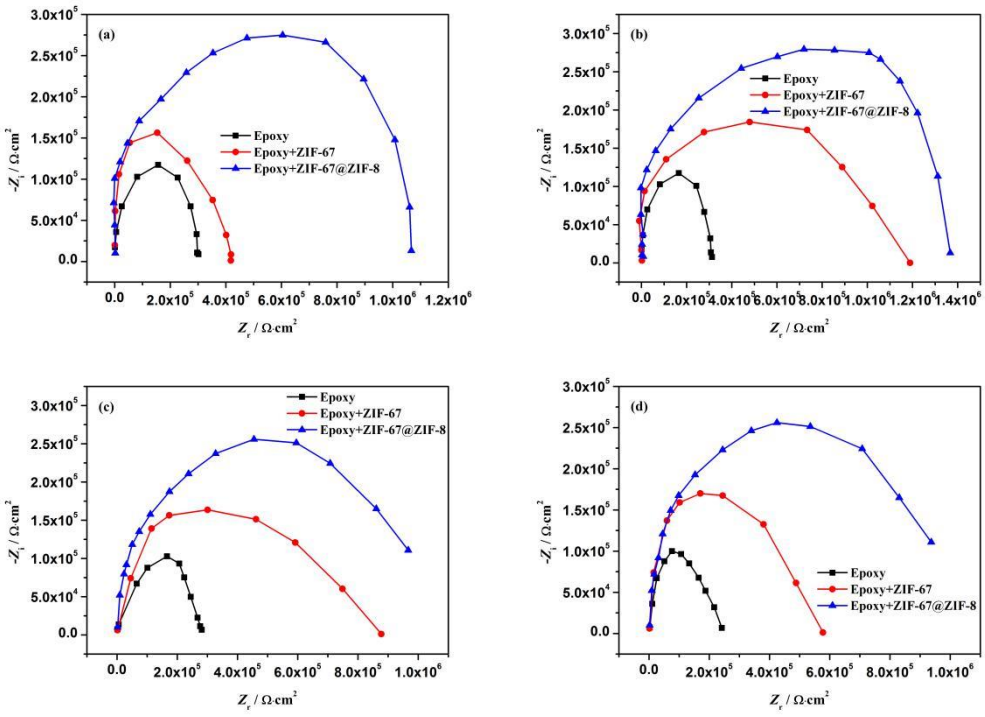

Figure 4. Nyquist plots of AZ31B immersed in 1 M HCl without or with ZIF nanoparticles for immersion times of (a) 1 h, (b) 24 h, (c) 48 h, (d) 120 h

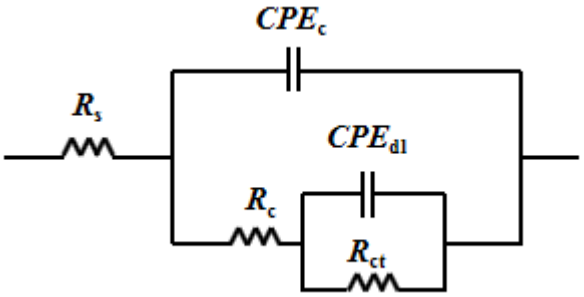

Figure 5. Equivalent circuit of EIS plots

Table 1. EIS parameters of AZ31B immersed in 1 M HCl with or without ZIF nanoparticles

Coating	Immersing time	Rs ($\Omega\cdot cm^2$)	Rc ($\Omega\cdot cm^2$)	CPE_c		R_{ct} ($\Omega\cdot cm^2$)	CPE_{dl}	
				Y_0 ($\mu F\cdot cm^{-2}$)	n		Y_0 ($\mu F\cdot cm^{-2}$)	n
Epoxy	1 h	35.2	3652	150.9	0.8	2.9×10^5	350.9	0.8
	24 h	34.4	3021	134.6	0.8	3.1×10^5	334.6	0.8
	48 h	51.8	1236	222.9	0.8	2.6×10^5	322.9	0.8
	120 h	63.4	996.5	312.2	0.8	2.2×10^5	312.2	0.8
Epoxy-ZIF-67	1 h	30.3	3895	126.8	0.8	4.2×10^5	437.5	0.8
	24 h	32.0	3429	71.2	0.8	1.2×10^6	380.4	0.8
	48 h	49.3	3128	116.3	0.8	8.6×10^5	342.5	0.8
	120 h	53.9	1985	121.5	0.8	5.9×10^5	340.7	0.9
Epoxy-ZIF-67@ZIF-8	1 h	36.3	3798	80.2	0.8	1.1×10^6	483.4	0.8
	24 h	34.3	3561	39.5	0.8	1.4×10^6	476.6	0.8
	48 h	46.3	3205	71.3	0.8	1.1×10^6	432.1	0.9
	120 h	49.4	2497	94.3	0.8	9.5×10^5	370.6	0.9

The anti-corrosion performance of the ZIF-67@ZIF-8 nanoparticles epoxy coating was also correlated with those of other previously reported organic coatings. The results are presented in Table 2, revealing that the epoxy coating with ZIF-67@ZIF-8 nanoparticles shows a comparable or even better anticorrosion performance than the previously reported organic coatings.

Table 2. Comparison of the anticorrosion performance of epoxy coating with ZIF-67@ZIF-8 nanoparticles and other organic coatings

Functional additive / layer	Resin	Electrolyte solution	R_{ct} ($\Omega\cdot cm^2$)	Reference
APTES[a]	Epoxy	0.05M NaCl	6.36×10^8	[24]
DES coating[b]	Epoxy	3.5% NaCl	4.04×10^4	[25]
MAO coating[c]	Epoxy	3.5% NaCl	1.5×10^6	[26]
PEO coating[d]	Epoxy	0.5% NaCl	2.91×10^4	[27]

ZIF-67@APS[e]	Epoxy	3.5% NaCl	8.16×10^{10}	[28]
ZM[f]	Epoxy/PDMS	3.5% NaCl	1.02×10^{5}	[29]
PANI-HF+MRP[g]	Epoxy	3% NaCl	1.36×10^{8}	[30]
$Ti_3C_2T_x$ MXene	Epoxy	3.5% NaCl	4.52×10^{7}	[31]
ZIF-67@ZIF-8	Epoxy	3.5% NaCl	1.06×10^{6}	This work

[a] Aminopropyltriethoxysilane.

[b] DES was prepared by stirring the ChCl and urea mixture at 80°C in a mole ratio of 1:2.

[c] MAO coating process on Mg substrate was performed in a stainless steel chamber (as a cathode) using a DC current power source (600V, 2.5A, 750W). In this process, Mg alloy samples served as an anode and the process was done under constant 100mA/cm^2 current density for 10min. The coating process was performed in a phosphate base electrolyte solution containing Na_3PO_4 (5g/l) and KOH (2g/l) with cerium oxide (1~5g/l) as an additive.

[d] Plasma electrolytic oxidation.

[e] ZIF-67: Cobalt-based zeolitic imidazolate frameworks, APS: Aminopropyltriethoxysilane.

[f] Zinc molybdate.

[g] Hydrofluoric-acid-doped polyaniline+Mg-rich primers.

The results of the immersion test are shown in Fig. 6. The optical image of the pure epoxy coating (left picture) exhibited corrosion products in the whole scratch area, indicating that the whole scratch area was eroded by corrosive particles. The findings demonstrated that scratching the pure epoxy coating did not provide sufficient corrosion resistance. After addition of ZIF-67@ZIF-8 nanoparticles, the resulting modified epoxy coating showed better corrosion resistance than the pure epoxy coating, which is in good agreement with the EIS results.

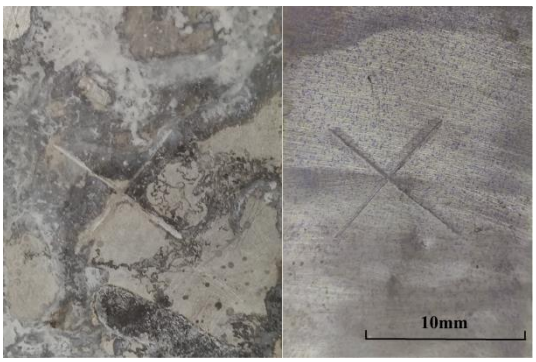

Figure 6. Optical images of artificial scratches obtained after immersion in 1 M HCl for 168 h

3.4 Anti-corrosion mechanism

Fig. 7 shows the anti-corrosion mechanism for the polymer coating on the surface of the metal. When cracking occured, the acidic corrosive medium quickly penetrated the coating along the scratch, as ZIF-67@ZIF-8 nanoparticles are pH responsive, and the corrosion inhibitor 2-MI was released from

ZIF-67@ZIF-8. Finally, the corrosion inhibitor formed a thin film in the fracture area, which acted as a dense barrier to prevent further corrosion of the metal.

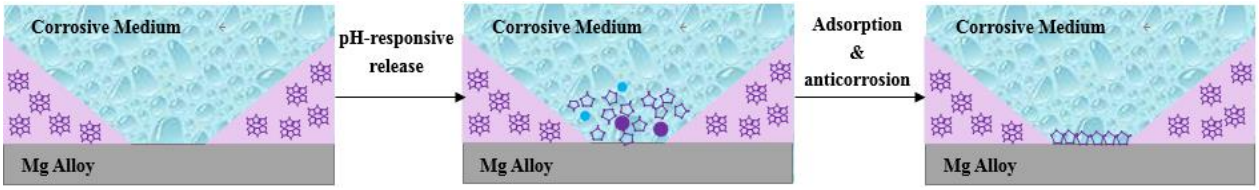

Figure 7. Schematic illustration of the anti-corrosion mechanism of the coating after addition of ZIF-67@ZIF-8 nanoparticles

4. CONCLUSION

ZIF-67@ZIF-8 nanoparticles can be used as controllable corrosion inhibitors in anticorrosive coatings. The corrosion inhibitor is released rapidly (more than 40%) in an acidic environment, while it is released slower and in smaller amounts (less than 4 wt%) in a neutral environment. In addition, under acidic conditions, the coating is doped with ZIF-67@ZIF-8. The excellent corrosion resistance of the coating may be due to the development of a reliable inhibitor adsorption film on the crack surface after exposure to the surrounding acidic environment.

ACKNOWLEDGEMENTS
The authors gratefully acknowledges the support of the National Natural Science Foundation of China (51708541), the Open Fund of Shandong Key Laboratory of Corrosion Science (KLCS201901); and the Opening Project of Material Corrosion and Protection Key Laboratory of Sichuan province (2019CL14).

References

1. N.E.L. Saris, E. Mervaala, H. Karppanen, J.A. Khawaja, A. Lewenstam, *Clin. Chim. Acta,* 294 (2000) 1.
2. M.P. Staiger, A.M. Pietak, J. Huadmai, G. Dias, *Biomater.,* 27 (2006) 1728.
3. C. Fox, D. Ramsoomair, C. Carter, *South. Med. J.,* 94 (2001) 1195.
4. B. Heublein, R. Rohde, V. Kaese, M. Niemeyer, W. Hartung, A. Haverich, *Heart,* 89 (2003) 651.
5. M. Esmaily, J.E. Svensson, S. Fajardo, N. Birbilis, G.S. Frankel, S. Virtanen, R. Arrabal, S. Thomas, L.G. Johansson, *Prog. Mater. Sci.,* 89 (2017) 92.
6. F.Y. Cao, G.L. Song, A. Atrens, *Corros. Sci.,* 111 (2016) 835.
7. S. Heise, S. Virtanen, A.R. Boccaccini, *J. Biomed. Mater. Res. Part A,* 104 (2016) 2628.
8. H.K. Singh, K.V. Yeole, S.T. Mhaske, *Chem. Eng. J.,* 295 (2016) 414.
9. C.G. Wang, L.P. Wu, F. Xue, R.Y. Ma, I.I.N. Etim, X.H. Hao, J.H. Dong, W. Ke, *J. Mater. Sci. Technol.,* 34 (2018) 1876.
10. X.P. Lu, Y. Li, P.F. Ju, Y. Chen, J.S. Yang, K. Qian, T. Zhang, F.H. Wang, *Corros. Sci.,* 148 (2019) 264.

11. A. Tan, A. Soutar, I. Annergren, Y. Liu, *Surf. Coating. Technol.,* 198 (2005) 478.
12. S. Zheng, J. Li, *J. Sol. Gel Sci. Technol.,* 54 (2010) 174.
13. X. Lu, S.P. Sah, N. Scharnagl, M. Stormer, M. Starykevich, M. Mohedano, C. Blawert, M.L. Zheludkevich, K.U. Kainer, *Surf. Coating. Technol.,* 269 (2015) 155.
14. M. Yoon, R. Srirambalaji, K. Kim, *Chem. Rev.,* 112 (2012) 1196.
15. M.G. Campbell, D. Sheberla, S.F. Liu, T.M. Swager, M. Dinca, *Angew. Chem.,* 54 (2015) 4349.
16. I. Stassen, M. Styles, G. Grenci, H. Van Gorp, W. Vanderlinden, S. De Feyter, P. Falcaro, D. De Vos, P. Vereecken, R. Ameloot, *Nat. Mater.,* 15 (2016) 304.
17. R. Sakamoto, *Bull. Chem. Soc. Jpn.,* 90 (2017) 272.
18. *J.C. Zhang, T.C. Zhang, K.S. Xiao, S. Cheng, G. Qian, Y. Wang, Y. Feng, Cryst. Growth Des.,* 16 (2016) 6494.
19. A. Phan, C.J. Doonan, F.J. Uribe-Romo, C.B. Knobler, M. O'Keeffe, O.M. Yaghi, *Acc. Chem. Res.,* 43 (2010) 58.
20. H. Furukawa, K.E. Cordova, M. O'Keeffe, O.M. Yaghi, *Science,* 341 (2013) 974.
21. P.F. Gao, L.L. Zheng, L.J. Liang, X.X. Yang, Y.F. Li, C.Z. Huang, *J. Mater. Chem. B,* 1 (2013) 3202.
22. R. Abazari, A. Reza Mahjoub, A.M.Z. Slawin, C.L. Carpenter-Warren, *Ultrason. Sonochem.,* 42 (2018) 594.
23. D. Wang, J. Zhou, R. Chen, R. Shi, G. Zhao, G. Xia, R. Li, Z. Liu, J. Tian, H. Wang, Z. Guo, H. Wang, Q. Chen, *Biomaterials,* 100 (2016) 27.
24. F. Brusciotti, D.V. Snihirova, H.B. Xue, M.F. Montemor, S.V. Lamaka, M.G.S. Ferreira, *Corros. Sci.,* 67 (2013) 82.
25. L.T.Guo, C.D. Gu, J. Feng, Y.B. Guo, Y. Jin, J.P. Tu, *J. Mater. Sci. Technol.,* 37 (2020) 9.
26. M. Toorani, M. Aliofkhazraei, R. Naderi, *J. Alloy. Compd.,* 785 (2019) 669.
27. M. Toorani, M. Aliofkhazraei, M. Mahdavian, R. Naderi, *Corros. Sci.,* 169 (2020) 108608.
28. S.M. Lashgari, H. Yari, M. Mahdavian, B. Ramezanzadeh, G. Bahlakeh, M. Ramezanzadeh, *Corros. Sci.,* 178 (2021) 109099.
29. U. Eduok, J. Szpunar, *Ultrason. Sonochem.,* 44 (2018) 288.
30. X.G. Feng, C. Zhu, X.Y. Lu, Y.J. Zhang, T. Wu, Y. Zuo, X.H. Zhao, Y.C. Dun, M. Wang, *Prog. Org. Coat.,* 141 (2020) 105550.
31. H. Yan, M. Cai, J.C. Wang, L. Zhang, H. Li, W. Li, X.Q. Fan, M.H. Zhu, *Appl. Surf. Sci.,* 536 (2021) 147974.